

# Soft Matter

Accepted Manuscript



This is an *Accepted Manuscript*, which has been through the Royal Society of Chemistry peer review process and has been accepted for publication.

*Accepted Manuscripts* are published online shortly after acceptance, before technical editing, formatting and proof reading. Using this free service, authors can make their results available to the community, in citable form, before we publish the edited article. We will replace this *Accepted Manuscript* with the edited and formatted *Advance Article* as soon as it is available.

You can find more information about *Accepted Manuscripts* in the [Information for Authors](#).

Please note that technical editing may introduce minor changes to the text and/or graphics, which may alter content. The journal's standard [Terms & Conditions](#) and the [Ethical guidelines](#) still apply. In no event shall the Royal Society of Chemistry be held responsible for any errors or omissions in this *Accepted Manuscript* or any consequences arising from the use of any information it contains.

# Suppression of Leidenfrost effect via low frequency vibrations

Boon T. Ng, Yew M. Hung, and Ming K. Tan\*

Received Xth XXXXXXXXXXXX 20XX, Accepted Xth XXXXXXXXXXXX 20XX

First published on the web Xth XXXXXXXXXXXX 200X

DOI: 10.1039/b000000x

The ability to suppress Leidenfrost effect is of significant importance in applications that require rapid and efficient cooling of surfaces with temperature higher than Leidenfrost point  $T_{SL}$ . Leidenfrost effect will result in substantial reduction in cooling efficiency and hence there have been a few different approaches to suppress the Leidenfrost effect. The majority of these approaches relied on fabricating micro/nano-structures to the heated surfaces, others relied on inducing electric field between the droplets and the heated surfaces. In this paper, we present an approach that induces low frequency vibrations ( $f \sim 10^2$  Hz) on the heated surface to suppress the effect. By mapping the different magnitudes of surface acceleration  $\ddot{\xi}_s$  versus different initial surface temperatures  $T_s$  of the substrate, three regimes that represents three distinct impact dynamics are analyzed. Regime-I represents gentle film boiling ( $\ddot{\xi}_s \sim 10^2$  m/s<sup>2</sup> and  $T_s \sim T_{SL}$ ), which is associated with the formation of thin spreading lamella around the periphery of the impinged droplet; Regime-II ( $\ddot{\xi}_s \sim 10^2$  m/s<sup>2</sup> and  $T_s > T_{SL}$ ) represents film boiling, which is associated with the rebound of the impinged droplet due to the presence of thick vapor layer; Regime-III ( $\ddot{\xi}_s \sim 10^3$  m/s<sup>2</sup> and  $T_s \sim T_{SL}$ ) represents contact boiling, which is associated with the ejection of tiny droplets due to the direct contact between the droplet and the heated surface. The estimated cooling enhancement for Regime-I is between 10% and 95%, Regime-II is between 5% and 15%, and Regime-III is between 95% and 105%. The improvement in cooling enhancement between Regime-I (strong Leidenfrost effect) and Regime-III (suppressed Leidenfrost effect) is more than 80%, demonstrating the effectiveness of using low frequency vibrations to suppress the Leidenfrost effect.

## 1 Introduction

When a small droplet is placed on the surface of a heated substrate, whose temperature is significantly higher than the boiling point of the liquid, a thin vapor layer is formed between the droplet and the substrate. This thin vapor layer is generated due to the initial intense evaporation when the droplets are in contact with the heated substrate. When the vapor pressure is sufficiently high to support the weight of the droplet, it prevents the droplets from contacting the heated surface directly. This phenomenon is known as the Leidenfrost effect;<sup>1</sup> it is also known as *film* boiling regime in a typical boiling process. The minimum temperature at which the Leidenfrost effect occurs is known as the Leidenfrost point/temperature.<sup>2</sup> A Leidenfrost droplet makes an almost 180 degree *contact* angle on the heated substrate, and hence the droplet cannot pin on the substrate, achieving a perfect nonwetting state. A few of the interesting phenomena based on the Leidenfrost effect have been reported:<sup>3</sup> self propelled Leidenfrost droplets,<sup>4–7</sup> drag reduction,<sup>8</sup> and suppression of Leidenfrost effect to improve heat transfer. The suppression of Leidenfrost effect, or the increase of Leidenfrost temperature, has recently garnered an increasing interest in the literature. The Leidenfrost effect

substantially reduces cooling efficiency due to the presence of a thin vapor layer, which prevents direct contact between the coolant and the hot surface. Consequently, it is highly non-desirable for high temperature cooling systems such as spray cooling system to have this effect. In this paper, our focus is on the suppression of Leidenfrost effect via low frequency vibrations.

Generally, the techniques to increase Leidenfrost temperature can be categorized into passive and active, as shown in Table 1. The passive techniques rely mostly on modifying the surface condition of the heated plate by either fabricating a thin layer of microstructure<sup>9–12</sup> or depositing a thin layer of nanofiber.<sup>13–18</sup> Passive techniques, on the other hand, do not require external force to elevate the Leidenfrost point. For instance, Kim *et al.*<sup>19</sup> conducted a detailed experimental study to investigate the parameters—roughness height, wettability, and porosity—that gives rise to a higher Leidenfrost point with the presence of microstructures on the heated plate. Surface roughness height was controlled by fabricating cylindrical microposts of 15  $\mu\text{m}$  height and 5  $\mu\text{m}$  diameter on a smooth silicon wafer. Subsequently, the surface wettability was controlled by depositing a nano-smooth layer of gold (100 nm thick). Finally, a thin nanoporous layer (600 nm thick) was deposited to study the effect of nanoporosity. In the experiment, they observed thin liquid filaments intermittently connecting the droplet to the substrate surface with the

School of Engineering, Monash University Malaysia, Jalan Lagoon Selatan, 47500 Bandar Sunway, Selangor, Malaysia; E-mail: [tan.ming.kwang@monash.edu](mailto:tan.ming.kwang@monash.edu)

microposts. The gold surface without nanoporosity can sustain the liquid filaments for a few milliseconds. With the presence of nanoporous surfaces, at locations where filaments were formed, violent splashes of tiny droplets around the large evaporating droplet were observed, preventing the establishment of a stable vapor layer between the droplet and the substrate. Essentially, liquid filaments begin to form when the height of the microposts is same as the thickness of the vapor layer. Once the filaments are established, heterogeneous nucleation of bubbles can occur at the contact points, if there are cavities (nanoporous) available for nucleation. This is due to the fact that bubbles are more easily nucleated on the nanoporous surface.

Unlike the passive techniques, which involve microfabrication to alter the condition of the heated surface by either using an array of microstructure or pre-depositing with a layer of nanofibers, for the active techniques, on the other hand, rely on externally induced force to break the vapour layer.<sup>7</sup> Celestini and Kirstetter<sup>20</sup> reported the method of applying electric field to the Leidenfrost droplet. In their study, vapor pocket below the Leidenfrost droplet was reduced by applying electric field between the droplet and the heated plate; electric field in the droplet induced capacitive force which then pulled the droplet towards the grounded plate. The vapor layer sandwiched between the droplet and the plate is eventually suppressed by further increasing the electric field. Although the applied voltage is quite low ( $\sim 10^1$  V), in an actual spray cooling process, it would be impossible for every single droplet to be connected to the electrode. In a different study by Deng and Gomez,<sup>21</sup> charged droplets generated by electrospray were employed to suppress the Leidenfrost effect. When charged droplets move close to the surface of the (grounded) heated plate, the droplets are attracted to the surface of the plate. To ensure the effectiveness of the technique, the impact time must be less than the charge relaxation time such that a sufficient number of charges are retained in the droplet after impact, then transferred to the grounded plate. We note here that for DC electrospray, the solution needs to have a lower surface tension coefficient than that of water ( $\gamma < \gamma_w$ ) and a certain level of electric conductivity  $K \sim 10^{-5}$  S/m.

In this work, we introduce a different approach to increase the Leidenfrost point by inducing a low frequency vibration ( $f \sim 10^2$  Hz) with accelerations within the range  $\xi_s \sim 10^2 - 10^3$  m/s<sup>2</sup> on the heated plate, resulting an increase of the impact force between the droplet and the heated plate. This proposed technique can be classified as one of the active techniques since it involves an external force to induce the vibrations. Nonetheless, contrary to AC electric field and electrospray technique as listed in Table 1, the proposed technique offers a few advantages such as no electric potential is required to apply across individual droplet (AC electric field), and deionised water can be used as coolant. We illustrate the

experimental setup in the following section, examine the dynamics of a falling droplet impinging on a heated and vibrating surface using high speed imaging, and demonstrate the effectiveness of the approach through temperature measurements.

## 2 Experimental Setup

The experiment work is divided into two parts: (1) high speed video recording for a single-droplet impinges on the heated static/vibrating plate, (2) quantifying the improvement of cooling efficiency by dispensing a continuous stream of droplets impinging on the heated static/vibrating plate. Figure 1 shows the general experimental setup. Briefly, the system consists of a vibrating plate driven by a loudspeaker. The vibrating plate was made of copper and the plate thickness was approximately 500  $\mu$ m. Sinusoidal waves within the frequency range from 100 to 250 Hz, were generated using a function generator (WF 1966, NF Corporation, Yokohama), and amplified using a variable amplifier to control the total power delivered to the loudspeaker. Two key parameters were changing in the experiments: surface temperature  $T_s \sim 150 - 250^\circ\text{C}$  and acceleration  $\xi_s \sim 10^0 - 10^2$  m/s<sup>2</sup> of the copper plate. In order to quantify the surface acceleration  $\xi_s$  of the plate, a low frequency laser Doppler Vibrometer (LDV) (Vibromet500V, MetroLaser, California) was employed; the surface acceleration of the plate was controlled by varying the plate surface displacement, which can be controlled by adjusting the power input to the loudspeaker. To elevate the surface temperature of the plate, a cylindrical-shape resistance-heater that connected to a high voltage power supply (PS 8160-04T, Elektro-Automatik, Viersen), was embedded within the periphery of the plate; this was done by drilling slots of cylindrical shape with a tight fit clearance to ensure effective heat transfer from the heat source to the copper plate. To control the surface temperature of the plate  $T_s$ , we employed a variable voltage controller, which was connected with the resistance heater. The temperature on the surface of the plate was measured using a T-type thermocouple that was soldered on the plate using a high melting point solder (83113090, RS, Selangor), and the temperature readings were recorded using a data logger (GL820, Graphtec, California) at a sampling rate of two recordings per second. Prior to each measurement, the plate was heated to the desired temperature and the surface temperature  $T_s$  of the plate was monitored to ensure the plate reached its steady-state condition.

In part (1) of the experimental study, i.e., high speed video recording for a single-droplet impinged on the heated static/vibrating plate, a 9- $\mu$ l droplet was dispensed from a needle that connected to a syringe filled with deionised water. The droplet detached from the needle tip when the gravitational pull became larger than the surface tension. A fixed distance of 20 mm between the tip of the needle and the surface

**Table 1** Summary of reported techniques to suppress Leidenfrost effect, i.e., to increase the Leidenfrost point. Generally, the techniques can be grouped into two different categories: passive and active technique. Note that  $D_0$  refers to the diameter of the impinging droplet.

	Technique	$D_0$	Brief description and key finding
Passive	Micro-nano structures <sup>9–12</sup>	$\sim 10^{-3}$ m	Pre-fabricate microstructure (of cylindrical or rectangular shape) array on the heated plate. The Leidenfrost point can be increased by adjusting the height and spacing between the microstructures; sparser array gives higher Leidenfrost point.
	Nanofiber coating <sup>13–15</sup>	$\sim 10^{-3}$ m	Pre-deposition of nanofiber on the heated surface, to generate a thin layer of fiber mat.
Active	Electrospray <sup>20</sup>	$\sim 10^{-5}$ m	Use electrospray technique to generate a plume of charged micro-droplets to impinge on the (grounded) heated plate. For heated plate above the Leidenfrost point, the image force causes the impinging droplet to stick on the heated plate.
	AC electric field <sup>21</sup>	$\sim 10^{-3}$ m	Apply a low frequency ( $\sim 10^0$ Hz) AC electric field ( $\sim 10^1$ V) across the droplet and the heated plate. The thickness of the vapour layer is proportional to the square of the applied voltage, i.e., $h_v \sim V^2$ .

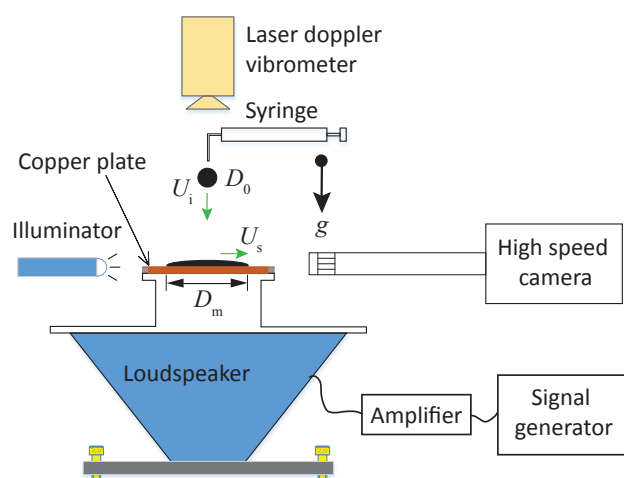


**Fig. 1** (Color online) A sketch illustrates the general experimental setup. A syringe is dispensing tiny droplet that impinges on the vibrating plate. A high speed camera, together with a high intensity illuminator, are used to record the complex interaction between the heated plate and the falling droplet. The sketch is not to scale.

of the plate was maintained throughout all experiments. A detailed interaction between the droplet and the plate was captured using a high speed camera (M310, Phantom, New Jersey) equipped with a long distance magnifying lens (1-50486, Navitar, Rochester, USA) to provide a maximum magnification of 40 times. A high intensity illuminator (41723-series, Cole Parmer, Malaysia) was used in the back-lighting imaging method to ensure sufficient contrast between the background and the droplet during the impact. The recorded im-

ages were then processed to extract various important parameters such as the drop diameter  $D_0$ , maximum spreading diameter  $D_m$ , impact velocity  $U_i$ , rebound velocity  $U_b$ , and lamella velocity  $U_s$ , as labelled in Figure 1. The interaction between the droplet and the vibrating substrate was captured when the falling droplet impinged on the vibrating plate that was moving in the upward direction.

In part (2) of the experimental study, a continuous stream of droplets was generated by connecting the dispenser with a controllable syringe pump (EW-74900-05 series, Cole Parmer, Malaysia). The dispensing rate was 1.1 ml/min. In order to quantify the effectiveness of the proposed technique to suppress Leidenfrost effect, which should lead to a better cooling efficiency, cooling enhancement ratio (CER) was used as a performance indicator. Starting from the Newton's law of cooling,  $\dot{Q} = hA(T_s - T_\infty)$ , the convective heat transfer coefficient can be expressed as  $h = (q'')/(T_s - T_\infty)$ , where  $q'' = \dot{Q}/A$  is the heat flux,  $A$  is the surface area of the heated plate,  $T_s$  is the surface temperature of the plate and  $T_\infty$  is the ambient temperature. By keeping the heat flux as a constant, the cooling enhancement ratio is thus defined as a ratio of the convective heat transfer coefficient with the presence of the droplet stream  $h_d$ , over that of the case without the droplet stream  $h_0$ , i.e.,

$$\text{CER} = \frac{h_d}{h_0} = \frac{T_0 - T_{0,\infty}}{T_d - T_{d,\infty}}, \quad (1)$$

where  $T_0$  is the steady state temperature of the plate without droplet stream,  $T_{0,\infty}$  is ambient temperature without droplet stream,  $T_d$  is the steady state temperature of the plate with droplet stream, and,  $T_{d,\infty}$  is ambient temperature with droplet stream. Higher enhancement ratio indicates higher cooling

rate.

Prior to the experimental studies, the static Leidenfrost point  $T_{SL}$ —deionised water droplet impinged on a static plate—was determined using our experimental setup as illustrated in Figure 1. The surface of the vibrating plate was polished using a polishing wax (D-42655, Autosol, Solingen, Germany), followed by rinsing using pure acetone to remove residues on the surface. We note here that the surface polishing and cleansing were applied to all the experiments in parts (1) and (2) of the experimental study as discussed above. Based on the recorded images (not shown), for our experimental setup, the static Leidenfrost point  $T_{SL}$  for the deionised water droplet impinged on the static plate was estimated to be approximately 170°C.

### 3 Results and discussion

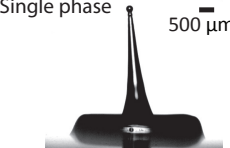
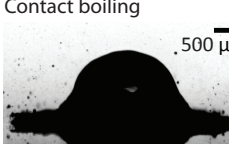
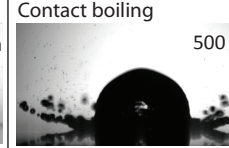
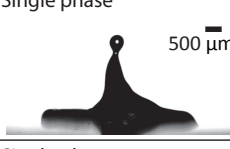
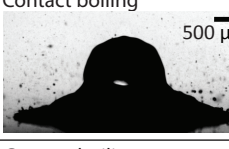
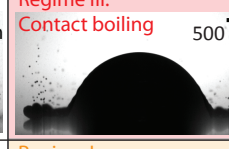
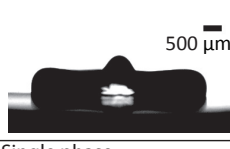
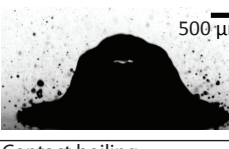
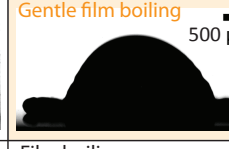
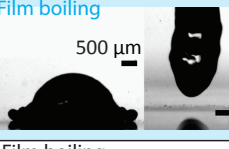
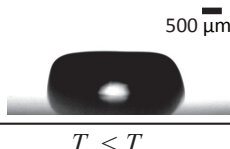
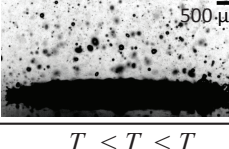
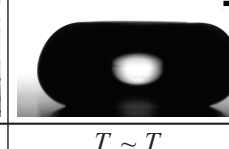
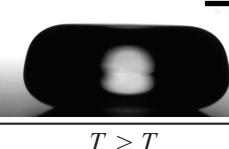
#### 3.1 Study of the dynamic of a falling droplet impinges on a heated vibrating plate via high speed recording

Figure 2 shows an overview of the interaction of a falling droplet on a stationary and vibrating substrate of surface acceleration between  $\xi_s \sim 0 - 10^3 \text{ m/s}^2$ , under four different ranges of surface temperature of the copper plate:  $T_s < T_b$  (below boiling point),  $T_b < T_s < T_{SL}$  (between boiling point and static Leidenfrost point),  $T_s \sim T_{SL}$  (at static Leidenfrost point), and  $T_s > T_{SL}$  (higher than static Leidenfrost point). When the surface temperature is below the boiling point of water, i.e.,  $T_s < T_b$ , the contact angle  $\theta_c$  between the impinged droplet and the heat plate is less than  $90^\circ$ , suggesting a full contact between the droplet and the plate. By increasing the surface acceleration, an elongated jet is formed. The heat transfer mechanism within this regime is single-phase. By increasing the surface temperature above the boiling point and below the static Leidenfrost point, i.e.,  $T_b < T_s < T_{SL}$ , we observed the ejection of tiny droplets, which is associated with bursting of vapor bubbles at the liquid-gas interface as a consequence of the contact boiling. By increasing the surface acceleration, the spreading lamella is becoming thinner. With further increase of surface temperature to that higher than static Leidenfrost point, i.e.,  $T_s \geq T_{SL}$ , on the static plate, we observed the contact angle is much larger than  $90^\circ$ , suggesting the formation of a thin vapor layer between the droplet and the heated surface, which is known as film boiling. By generating vibrations on the heated plate at  $T_s \sim T_{SL}$ , the film boiling regime is transitioning to *gentle* film boiling when  $\xi_s \sim 10^2 \text{ m/s}^2$  (Regime I), and to contact boiling with ejection of tiny droplets when  $\xi_s \sim 10^3 \text{ m/s}^2$  (Regime III), and finally to contact boiling with disintegration of spreading lamella when  $\xi_s > 10^3 \text{ m/s}^2$ . We note here that the gentle film boiling<sup>22</sup> is referred to the presence of a thin vapor layer that prevents a direct contact between the droplet and the heated surface. Further increas-

ing the surface temperature of the plate, i.e.,  $T_s > T_{SL}$ , gentle film boiling with bouncing was observed when  $\xi_s \sim 10^2 \text{ m/s}^2$  (Regime II). Regime I, II and III are the focus of this work.

**3.1.1 Regime I: Gentle film boiling** In this regime, a thin spreading lamella is forming around the periphery of the impinged droplet. The surface temperature  $T_s$  of the plate was varied in the range from 160 to 190°C ( $T_s \sim T_{SL}$ ), whereas the acceleration of the plate was varied within the order of  $10^2 \text{ m/s}^2$ . Figures 3(a) and (b) show the sequential images of the droplet impinged on the stationary and vibrating plate, respectively. Due to the motion of the heated plate, the thickness of the lamella was reduced at higher surface acceleration. The dynamic of spreading lamella is analyzed by comparing the forces that exert on the impinged droplet and the Weber number of the spreading lamella. Two significant forces that the droplet experiences when impinging on the heated plate are the impact force  $F_I$  and the vapor force  $F_v$ ; the former is caused by higher collision force due to the motion of the plate, and the latter is caused by the rapid formation of vapor layer between the droplet and the plate. The impact force is estimated as  $F_I \equiv \rho R_m^2 (U_i + \xi_s f^{-1})^2$ , where  $\rho$  is the density of the liquid,  $R_m$  is the maximum spreading radius of the lamella,  $U_i$  is the impact velocity,  $\xi_s$  is the surface acceleration of the plate, and  $f$  is the vibration frequency of the plate. On the other hand, the vapor force is estimated as  $F_v \equiv p_v R_m^2$ , where  $p_v$  is the vapor/saturated pressure. The Weber number for the spreading lamella can be estimated as  $We_l \equiv \rho U_s^2 R_m / \gamma$ , where  $U_s$  is the velocity of the spreading lamella, and  $\gamma$  is the surface tension of the liquid. In the experiments,  $F_I$  and  $F_v$  were varied by using different plate vibration acceleration  $\xi_s$  and plate surface temperature  $T_s$ . All the experimental data were found to collapse to a single line representing a linear relationship between the Weber number of the spreading lamella and the ratio of the forces, i.e.,  $We_l \sim F_I / F_v$ , as shown in Fig. 3(c). Not surprisingly, increasing the inertial force of the impinged droplet leads to higher Weber numbers for the spreading lamella, resulting in larger  $R_m$ . Nonetheless, by increasing the temperature of the plate (thus increases the vapor pressure  $p_v$  which leads to higher  $F_v$ ), the Weber number is reduced, resulting in smaller  $R_m$ . Therefore, in order to achieve a larger spreading radius  $R_m$  (hence to enhance the heat transfer) the impact force should increase whereas the vapor force should reduce. The reduction of  $We_l$  as the temperature of the plate increases is attributed to the higher viscous stress  $\tau$  exerted by the vapor layer on the liquid-vapor interface, i.e.,  $\tau \sim \mu_v U_s / h_v$ , where  $\mu_v$  is the viscosity of the vapor and  $h_v$  is the thickness of the vapor layer. For gaseous medium, the viscosity increases with increased temperature, leading to higher viscous stress and reducing the inertial force of the spreading lamella.

We recast the experimental data to plot the relationship between the maximum spreading  $D_m/D_0$  and the Weber num-

Surface acceleration $\ddot{\xi}_s$ (m/s <sup>2</sup> )	$\ddot{\xi}_s > 10^3$ ( $\zeta_s > 100g$ )	Single phase  500 $\mu\text{m}$	Contact boiling  500 $\mu\text{m}$	Contact boiling  500 $\mu\text{m}$	
	$\ddot{\xi}_s \sim 10^3$ ( $\zeta_s \sim 100g$ )	Single phase  500 $\mu\text{m}$	Contact boiling  500 $\mu\text{m}$	Regime III: Contact boiling  500 $\mu\text{m}$	
	$\ddot{\xi}_s \sim 10^2$ ( $\zeta_s \sim 10g$ )	Single phase  500 $\mu\text{m}$	Contact boiling  500 $\mu\text{m}$	Regime I: Gentle film boiling  500 $\mu\text{m}$	Regime II: Film boiling  500 $\mu\text{m}$
	$\ddot{\xi}_s \sim 0$ (Stationary plate)	Single phase  500 $\mu\text{m}$	Contact boiling  500 $\mu\text{m}$	Film boiling  500 $\mu\text{m}$	Film boiling  500 $\mu\text{m}$
		$T_s < T_b$	$T_b < T_s < T_{SL}$	$T_s \sim T_{SL}$	$T_s > T_{SL}$
		Surface temperature $T_s$			

**Fig. 2** (Color online) Various phenomena can be observed when a  $9\text{-}\mu\text{l}$  droplet impinges on a vibrating plate at different surface accelerations  $\ddot{\xi}_s$  and surface temperatures  $T_s$ . Note here that  $g$  refers to the gravitational acceleration,  $T_b$  refers to the boiling point, and  $T_{SL}$  refers to the static Leidenfrost point.

ber of the impinged droplet, which can be estimated as  $We_i \equiv \rho D_0 \left( U_i + \ddot{\xi}_s f^{-1} \right)^2 / \gamma$ , where  $D_0$  is the initial diameter of the droplet. Based on the fitted line (see Fig. 4), the result shows that  $D_m$  scales as  $We_i^{1/4}$ , consistent with the previously reported finding by Clanet *et al.*<sup>23</sup> on the impacting drop on a superhydrophobic/hydrophilic, stationary ( $\ddot{\xi}_s \sim 0$ ), and non-heated plate. In a different study reported by Tran *et al.*<sup>22</sup>, their result shows that for droplet impacting on a superheated surface ( $250^\circ\text{C} \leq T_s \leq 560^\circ\text{C}$ ), stationary ( $\ddot{\xi}_s \sim 0$ ), and at high impact velocity ( $0.5 \leq We_i \leq 600$ ), the relationship changes to  $D_m \sim We_i^{2/5}$ ; the steeper scale of  $2/5$  is attributed to the motion of vapor that moves radially outward, forming an additional drag force that assists the lamella spreading. More recently, Tran *et al.*<sup>24</sup> and Nair *et al.*<sup>14</sup> reported that for droplet impacting on the superheated ( $240^\circ\text{C} \leq T_s \leq 540^\circ\text{C}$ ), stationary ( $\ddot{\xi}_s \sim 0$ ) surface with microstructure/nanofiber, the relationship changes to  $D_m \sim We_i^{3/10}$ ; similarly, the steeper scale of  $3/10$  as compared to  $1/4$  is attributed to the drag that exerts on the liquid-vapor interface due to the motion of the vapor in the radially outward direction. Interestingly, in our experiment, although the plate was heated above the static Leidenfrost point, the data show the scaling relationship of  $1/4$  in-

stead of  $2/5$  or  $3/10$ . This result suggests that without superheating the plate, i.e.,  $T_s \gg T_{SL}$ , the dynamics of the spreading droplet is almost identical to the non-heating case; therefore, the vapor drag is insignificant. Table 2 shows a comparison between the reported studies and the current study on the dynamics of spreading lamella for droplet impacting on the plate under different conditions.

**3.1.2 Regime II: Film boiling** By increasing the surface temperature to slightly higher than the static Leidenfrost point, i.e.,  $T_s > T_{SL}$ , the impinged droplet on the vibrating plate is observed to rebound after the first impact. In our experiment, within this regime, the surface temperature of the plate is in the range of  $210^\circ\text{C} < T_s < 250^\circ\text{C}$  and the surface acceleration of the plate is in the order of  $\ddot{\xi}_s \sim 10^2 \text{ m/s}^2$ . Due to the higher surface temperatures, the vapor pressure  $p_v$  exerts on the impinged droplet increases, leading to the rebound of the droplet as shown in Fig. 5(a). We analyze the dynamics of droplet rebound by considering the dominant collision forces— $F_T = F_I + F_v$ , where  $F_T$  is the total force,  $F_I$  is the impact force and  $F_v$  is the vapor force—during the impact of the droplet with the vibration plate, and the Weber number of the rebounding droplet  $We_b \equiv \rho D_0 U_b^2 / \gamma$ , where  $U_b$  is the veloc-

**Table 2** Summary of the reported and current study on the scaling of maximum spread factor ( $D_m/D_0$ ) as a function of Weber number  $We_i$  under different conditions.

Reported by	Impacting drop	Surface condition	Surface motion	Surface temperature	Scaling
Clanet <i>et al.</i> <sup>23</sup>	$1 < We_i < 300$	Superhydrophobic/ hydrophilic	Stationary	Room temperature	$D_m/D_0 \sim We_i^{1/4}$
Tsai <i>et al.</i> <sup>25</sup>	$1 < We_i < 300$	With microstructures	Stationary	Room temperature	$D_m/D_0 \sim We_i^{1/4}$
Tran <i>et al.</i> <sup>22</sup>	$10 < We_i < 600$	Smooth	Stationary	$250^\circ\text{C} < T_s < 560^\circ\text{C}$	$D_m/D_0 \sim We_i^{2/5}$
Antonini <i>et al.</i> <sup>26</sup>	$1 < We_i < 100$	Smooth	Stationary	$T_s \sim 300^\circ\text{C}$	$D_m/D_0 \sim We_i^{2/5}$
Tran <i>et al.</i> <sup>24</sup>	$10 < We_i < 200$	With microstructures	Stationary	$240^\circ\text{C} < T_s < 540^\circ\text{C}$	$D_m/D_0 \sim We_i^{3/10}$
Nair <i>et al.</i> <sup>14</sup>	$2 < We_i < 320$	With nanofiber	Stationary	$60^\circ\text{C} < T_s < 450^\circ\text{C}$	$D_m/D_0 \sim We_i^{3/10}$
Current study	$60 < We_i < 200$	Smooth	$\ddot{\xi}_s \sim 10^2 \text{ m/s}^2$ $f \sim 10^2 \text{ Hz}$	$160^\circ\text{C} < T_s < 190^\circ\text{C}$	$D_m/D_0 \sim We_i^{1/4}$

ity of the rebounding droplet. By plotting  $We_b$  versus  $F_T$ , all the experimental data were able to collapse into a linear line, which indicates  $We_b \sim F_T$ , as shown in Fig. 5(b). Therefore, to prevent the rebound of the droplet from the vibrating plate, either the impact force  $F_I$  or the vapor force  $F_v$  has to be reduced. Due to the presence of thicker vapor layer that leads to the droplet rebound, in this regime, we expect the cooling enhancement should be weaker as compared to Regime-I. We note here that for Regime-I, droplet rebounding is possible when the surface acceleration is low; however, the contact time between the droplet and the plate—time between the impact and prior to the rebound—is twice that of the rebounding process in Regime-III.

**3.1.3 Regime III: Contact boiling** Within this regime, the surface temperature of the vibrating plate is  $T_s \sim T_{SL}$ , i.e.,  $160^\circ\text{C} < T_s < 190^\circ\text{C}$  based on our experiment setup, and the surface acceleration of the plate in the order of  $\ddot{\xi}_s \sim 10^3 \text{ m/s}^2$ . Essentially, the range of surface temperature is same as Regime-I, however, the surface acceleration is increased from  $\ddot{\xi}_s \sim 10^2 \text{ m/s}^2$  in Regime-I to  $\ddot{\xi}_s \sim 10^3 \text{ m/s}^2$  in Regime-III. This increase of surface acceleration of the plate causes higher collision forces between the impinged droplet and the plate, leading to a direct contact between the spreading lamella and the heated plate. The direct contact between the lamella and the heated plate results in nucleate boiling, i.e., the formation of vapor bubbles, and subsequently the ejection of tiny droplets (see Fig. 6(a)) of diameter in the order of  $d_e \sim 10^{-5} \text{ m}$  as a consequence of bursting of these vapor bubbles at the liquid-air interface.<sup>27–29</sup> We note that the critical radius for an embryonic vapor bubble can be approximated by  $R_c = 2\gamma/(p_v - p_\infty)$ ,<sup>30</sup> where  $p_\infty$  is the surrounding pressure.

For our experiment, the critical radius is estimated in the order of  $R_c \sim 10^{-7} \text{ m}$ , which is smaller than the thickness of the lamella ( $h_\ell \sim 10^{-6} \text{ m}$ ). The embryonic vapor bubble grows in the lamella and the maximum size it can attain is limited by the lamella thickness. Once the vapor bubble is burst, capillary waves are generated at the liquid-air interface and subsequently these waves converged, forming a tiny jet.<sup>31</sup> Figure 6(b) shows the formation of tiny jets—height  $h_j \sim 10^{-4} \text{ m}$  and diameter  $d_j \sim 10^{-6} \text{ m}$ —on the surface of the spreading lamella, which then break-up to form multiple droplets. The size of the ejected drops is on the same order as the diameter of the jet, i.e.,  $d_e \sim d_j \sim 10^{-6} \text{ m}$ . Due to the direct contact between the impinged droplet and the heated surface, in this regime, we expect the cooling enhancement should be the highest as compared to those of Regime-I and Regime-II.

## 3.2 Study of the cooling enhancement

By selecting the three regimes as outlined above (Regimes I, II, and III), in this section, we investigate the effectiveness of the technique to suppress the Leidenfrost effect by estimating the cooling enhancement ratio (CER), as shown in Equation (1). Prior to analyzing the vibration effect, a set of experiments to verify the measurement method was conducted by dispensing a continuous stream of droplets on a static plate at varying surface temperature. The result is shown in Figure 7, in which four different boiling regimes—natural convection boiling (single-phase), nucleate boiling, transition boiling, and film boiling—are identified. For the natural convection boiling regime, the surface temperature of the heated plate is below the boiling point for water ( $T_s \leq T_b$ ) and the heat transfer from

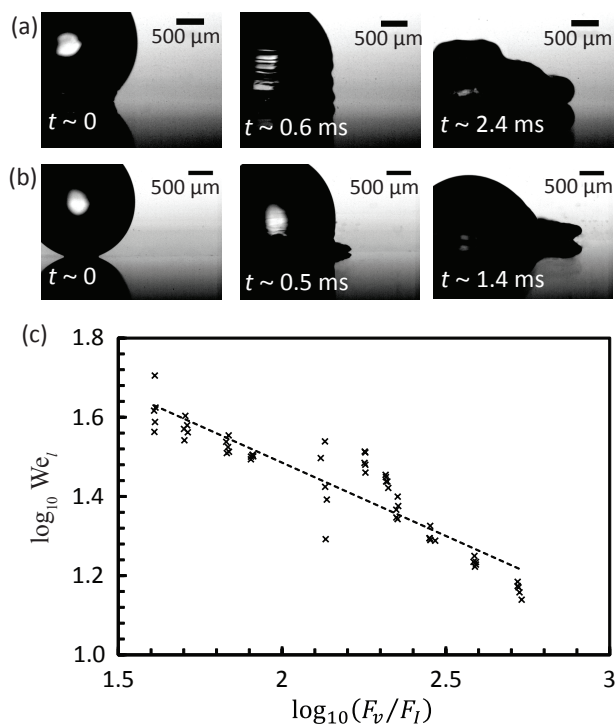


**Fig. 3** Sequential images recorded at 10000 frames per second show a 9- $\mu\text{l}$  droplet impinging on a heated (a) stationary, and (b) vibrating plate. For droplet impinged on a vibrating plate, a thinner lamella was observed to form around the periphery of the droplet. For each run, the maximum spreading radius  $R_m$  and the velocity of the spreading lamella  $U_s$  were measured, for the subsequent estimation of the lamella Weber number  $We_l$ . (c) The plot shows a linear relationship between the  $We_l$  and the ratio of vapor force  $F_v$  over the impact force  $F_I$ , i.e.,  $We_l \sim F_I/F_v$ .

the heated surface to the impinged liquid is by natural convection. Within this regime, the measured cooling enhancement ratio is maintained at approximately 1.2; that is 20% improvement in cooling with droplets impinged on the heated surface compared to cooling without droplet. We note that the natural convection boiling regime is extended slightly beyond the boiling point. Once the surface temperature increases higher than the boiling point to be within the nucleate boiling regime ( $T_b < T_s \leq T_c$ , where  $T_c$  refers to the point of critical heat flux), vapor bubbles are formed and the heat transfer from the heated plate to the impinged droplet is enhanced due to the effect of liquid entrainment and evaporation. At even higher surface temperatures ( $T_c < T_s \leq T_{SL}$ ), the cooling enhancement ratio reduces with increasing temperature caused by a larger fraction of the heated surface covered by the vapor bubble/film, which acts as an thermal insulator due to the low thermal conductivity of the vapor. The cooling enhancement ratio eventually drops to less than 1.1; that is only 10% improvement

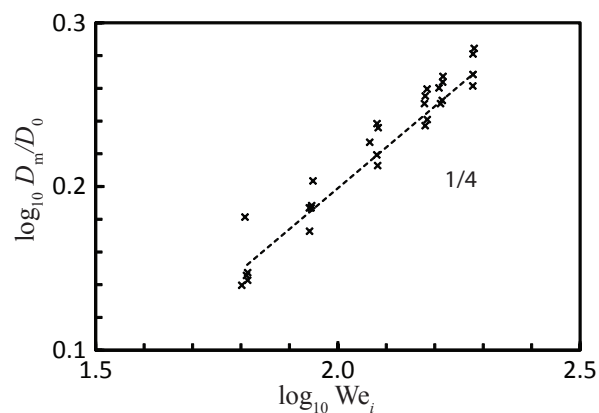


**Fig. 4** The plot shows the normalization of maximum spreading diameter  $D_m$  using the initial droplet diameter  $D_0$ , versus the Weber number of the falling droplet  $We_f$ . The surface temperature of the plate was between 160 and 190 $^{\circ}\text{C}$ , and the surface acceleration was in the order of  $10^2$   $\text{m/s}^2$ . The dotted line represents the best fit, which shows that  $D_m/D_0 \sim We_i^{1/4}$ .

in cooling with droplets impinged on the heated surface compared to cooling without droplet. By increasing the surface temperature of the plate to above the static Leidenfrost point ( $T_s > T_{SL}$ ), a continuous thin vapor layer is formed between the droplet and the heated substrate. Consequently, within this regime, the cooling enhancement is less than 10%. Overall, the results shown in Fig. 7 are consistent with the typical boiling curve for water.

With the introduction of low frequency vibrations ( $f \sim 10^2$  Hz), at the sufficient magnitude of surface acceleration, the cooling enhancement ratio is increased substantially, as shown in Figure 8. Again, three different regimes—Regime-I represents gentle film boiling, Regime-II represents film boiling, and Regime-III represents contact boiling—as outlined in Sec. 3.1 are selected for the study. In the experiments, for Regimes I and III, the initial surface temperature of the heated plate was 185 $^{\circ}\text{C}$  ( $T_s \sim T_{SL}$ ), whereas for Regime II, the initial surface temperature was 220 $^{\circ}\text{C}$  ( $T_s > T_{SL}$ ). We note here that for the initial surface temperatures of 185 $^{\circ}\text{C}$  and 220 $^{\circ}\text{C}$ , without vibrations ( $\xi_s \sim 0$ ), these two surface temperatures correspond to the condition of film boiling state with the CER less than 1.1, as shown in Figure 7.

Within Regime-I, the cooling enhancement ratio ( $1.1 < CER < 1.95$ ) increases linearly with increasing surface acceleration of the heated plate ( $220$   $\text{m/s}^2 < \xi_s < 1000$   $\text{m/s}^2$ ), consistent with the result shown in Fig. 3(c) for the linear relationship between Weber number of the spreading lamella  $We_l$  and the impact force  $F_I$ , i.e.,  $We_l \sim F_I$ . Therefore, the higher the impact forces, the larger the Weber numbers of the spreading lamella, leading to larger areas of the flatten



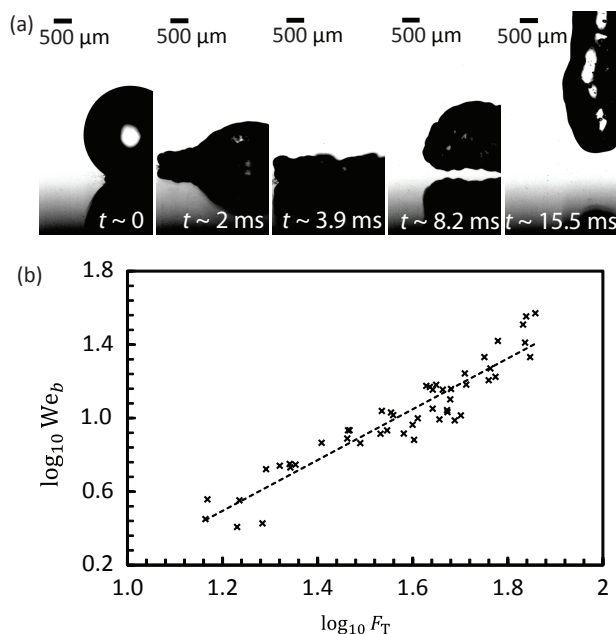


**Fig. 5** (a) Sequential images show the rebound of a  $9\text{-}\mu\text{l}$  droplet atop a heated ( $T_s \approx 230^\circ\text{C} > T_{SL}$ ) and vibrated plate ( $650\text{ m/s}^2$ ). The images were captured at a rate of 10000 frames per second. In the experiment, the surface acceleration of the plate was varied between  $200\text{ m/s}^2 < \xi_s < 850\text{ m/s}^2$ , whereas the surface temperature was varied between  $210^\circ\text{C} < T_s < 250^\circ\text{C}$ . (b) The relations between the Weber number of the rebounding droplet  $We_b$  and the total force during the impact  $F_T = F_I + F_v$ . The experimental data were able to collapse into a linear line, represented by the dotted line which shows that  $We_b \sim F_T$ .

droplets facing the heated surface, thus enhancing the heat transfer. Within Regime-II, the cooling enhancement ratios increase marginally ( $1.05 < CER < 1.15$ ) with surface acceleration varied within the range of ( $210\text{ m/s}^2 < \xi_s < 1420\text{ m/s}^2$ ). As discussed previously, Regime II represents the film boiling regime, wherein a relatively thick continuous layer of vapor is present between the droplet and the heated plate, facilitating the droplet rebound as shown in Figure 5(a) and reducing the transfer of heat from the heated surface to the droplet; there is only 5% to 15% of improvement in cooling. We note that the CERs for Regime II are in the same range as the film boiling state without vibrations (see Fig. 7), suggesting the presence of the vapor layer in retarding the heat transfer between the heated substrate and the droplets is still strongly felt. Within Regime-III, the measured cooling enhancement ratio is increased marginally from 1.95 to 2.05, with increasing surface acceleration from  $1000\text{ m/s}^2$  to  $1620\text{ m/s}^2$ . The results indicate that there exists a linear suppression range from  $\xi_s = 220\text{ m/s}^2$  to  $1000\text{ m/s}^2$  (Regime-I), and a plateau is obtained when the surface acceleration higher than  $1000\text{ m/s}^2$  (Regime-III).

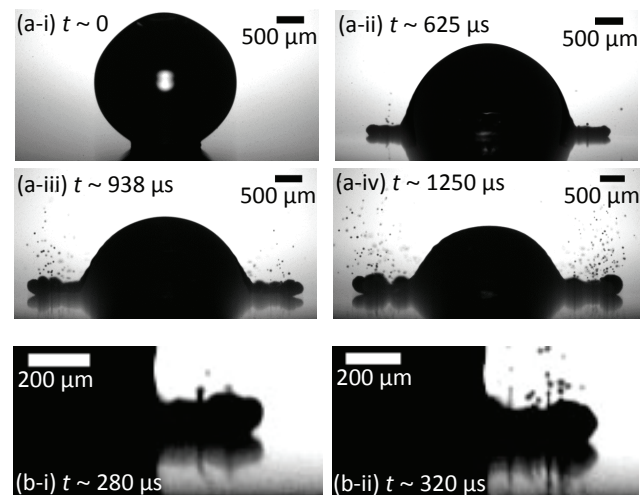


**Fig. 6** Sequential images recorded at 3200 frames per second, show a  $9\text{-}\mu\text{l}$  droplet impinging on a vibrating plate  $\xi_s \sim 10^3\text{ m/s}^2$ . The surface temperature of the plate was  $T_s \sim T_{SL}$ . Within this regime, (a) spreading lamella accompanied with ejection of tiny droplets was observed. (b) Close-up images recorded at higher frame rate of 25000 frames per second, show a clearer view of the ejection process, in which a tiny jet is formed and subsequently breakup into tiny droplets of diameter in the order of  $d_e \sim 10^{-5}\text{ m}$ .

Nonetheless, the improvement in cooling is twice of that of natural convection cooling. This is due to the direct contact between the droplet and the heated plate, resulting in the nucleation boiling within the thin lamella and leading to the generation of tiny droplets, as shown in Figure 6. The slight increase of CER from 1.95 to 2.05 is attributed to the small increase of diameter of the spreading lamella  $D_m$  as the surface acceleration increases. The Leidenfrost effect has been completely suppressed in Regime-III, i.e., the Leidenfrost point  $T_L$  has been increased to higher temperature.

Finally, by using two initial surface temperatures of the heated plate— $95^\circ\text{C}$  ( $T_s < T_b$ ) and  $185^\circ\text{C}$  ( $T_s > T_{SL}$ )—together with a constant dispensing rate of droplets at  $1.1\text{ ml/min}$ , the final surface temperatures of the heated plate were measured at different levels of surface acceleration. Figure 9 shows the measured final surface temperature of the heated plate versus surface acceleration. For the initial surface temperature of  $T_s \approx 95^\circ\text{C} < T_b$ , the final surface temperatures of the plate only drop a little from  $81^\circ\text{C}$  ( $\xi_s \sim 0$ ) to  $73^\circ\text{C}$  ( $\xi_s \sim 1220\text{ m/s}^2$ ). Since the initial surface temperature of the plate is below the boiling point, without vibrations ( $\xi_s \sim 0$ ), the heat is transferred to the droplet through natural convection boiling (single-phase). With the introduction of vibrations, the final plate surface temperature is slightly reduced due to the motions within the liquid that enhance the thermal transport. On the other hand, for the initial surface tempera-

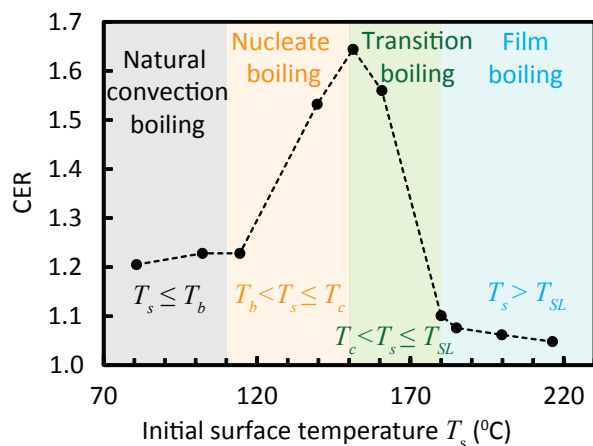


**Fig. 7** (Color online) Measured cooling enhancement ratio (CER) for the condition of a constant stream of droplets impinged on a stationary heated plate ( $\xi_s \sim 0$ ) at the rate of 1.1 ml/min. The initial surface temperature of the stationary plate was varied from below boiling point to above the static Leidenfrost point. A distinct four regions—natural convection boiling (single phase) ( $T_s \leq T_b$ ), nucleate boiling ( $T_b < T_s \leq T_c$ ), transition boiling ( $T_b < T_s \leq T_{SL}$ ), and film boiling ( $T_s > T_{SL}$ )—can be clearly identified and consistent with the standard boiling curve;  $T_s$  refers to surface temperature,  $T_b$  refers to boiling point,  $T_c$  refers to critical heat flux point, and  $T_{SL}$  refers to static Leidenfrost point. The dotted line was added to aid visualization.

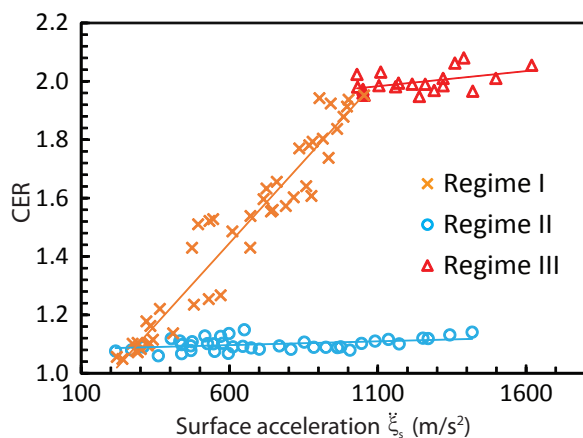


**Fig. 8** (Color online) Measured cooling enhancement ratio (CER) for a continuous stream of droplets impinged on a heated surface at different surface acceleration  $\xi_s$ . The results were grouped according to the regimes as defined in Fig. 2: (x) Regime-I represents gentle film boiling (initial  $T_s \approx 185^\circ\text{C}$  and  $220 \text{ m/s}^2 < \xi_s < 1000 \text{ m/s}^2$ ), (o) Regime-II represents film boiling (initial  $T_s \approx 220^\circ\text{C}$  and  $210 \text{ m/s}^2 < \xi_s < 1420 \text{ m/s}^2$ ), and, ( $\Delta$ ) Regime-III represents contact boiling (initial  $T_s \approx 185^\circ\text{C}$  and  $1000 \text{ m/s}^2 < \xi_s < 1620 \text{ m/s}^2$ ). The trend lines were added to aid visualization.

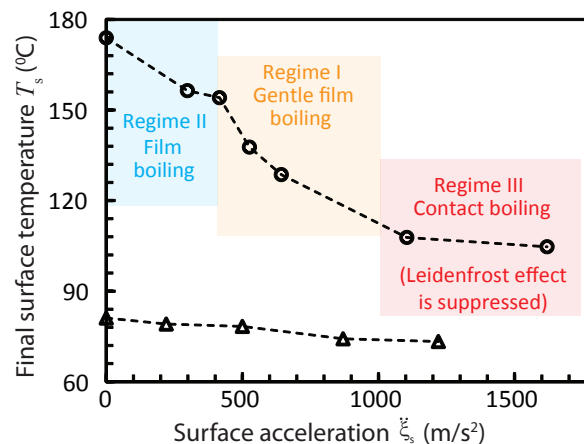


**Fig. 9** (Color online) Experimental results show the effect of surface acceleration  $\xi_s$  on the final surface temperature  $T_s$  of the heated plate. Two different initial surface temperatures were selected: ( $\Delta$ )  $95^\circ\text{C}$  (slightly below boiling point), and, ( $\circ$ )  $185^\circ\text{C}$  (slightly above static Leidenfrost point for stationary plate). The droplets were dispensed at the rate of 1.1 ml/min. The dotted lines were added to aid visualization.

ture of  $T_s \approx 185^\circ\text{C} > T_{SL}$ , the final surface temperatures of the plate drop substantially from  $174^\circ\text{C}$  (when  $\xi_s \sim 0$ ) to  $105^\circ\text{C}$  (when  $\xi_s \sim 1620 \text{ m/s}^2$ ). Using the phase-diagram shown in Fig. 10, for initial surface temperature of  $185^\circ\text{C}$ , we can divide the curve shown in Fig. 9 into three different regimes: Regime-II (film boiling) dominates when the surface acceleration is between  $0 \leq \xi_s < 400 \text{ m/s}^2$ , Regime-I (gentle film boiling) dominates when the surface acceleration is between  $400 \text{ m/s}^2 < \xi_s < 1000 \text{ m/s}^2$ , and Regime-III (contact boiling) dominates when the surface acceleration is larger than  $1000 \text{ m/s}^2$ . Therefore, at the initial surface temperature of  $185^\circ\text{C}$ , the Leidenfrost effect can be suppressed completely when the surface acceleration of the plate increases beyond  $1000 \text{ m/s}^2$ , leading to a  $80^\circ\text{C}$  drop of surface temperature; the final surface temperature is  $105^\circ\text{C}$ . This final surface temperature can be further reduced by increasing the dispensing rate of the droplets.

## 4 Conclusions

We presented the method to suppress Leidenfrost effect (or increase Leidenfrost point) by inducing vibrations on the heated surface. Different phenomena were observed and quantified through the mapping of the dynamic behavior of the impinged droplet on a heated surface at different magnitudes of surface acceleration. Three important regimes—gentle film boiling, film boiling, and contact boiling—which show three distinct dynamic behaviors of the impinged droplet—formation of thin spreading lamella around the periphery of the im-

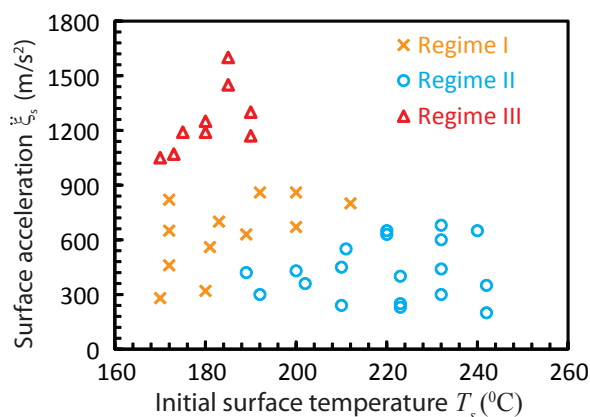


**Fig. 10** (Color online) Phase diagram shows the mapping of the droplet response—(×) Regime I represents gentle film boiling, (○) Regime II represents film boiling, and (△) Regime III represents contact boiling, as outlined in Fig. 2—on a vibrating plate at different magnitudes of surface acceleration  $\xi_s$  and surface temperature  $T_s$ .

pinged droplet, rebound of the impinged droplet, and ejection of tiny droplets, respectively—are selected for a more detailed analysis. Gentle film boiling occurs when the surface temperature of the heated plate is at the static Leidenfrost point ( $T_s \sim T_{SL}$ ) and the surface acceleration is in the order of  $\xi_s \sim 10^2$  m/s<sup>2</sup>. The estimated cooling enhancement ratio for cooling within gentle film boiling regime is between 1.1 and 1.95, i.e., between 10% and 95% increase in cooling as compared to the case of pure natural convection without droplets and vibrations. Film boiling occurs when  $T_s > T_{SL}$  and  $\xi_s \sim 10^2$  m/s<sup>2</sup>. The estimated cooling enhancement ratio for cooling within the film boiling regime is only between 1.05 and 1.15, indicating the effect of vibrations is insignificant, whereas the effect of vapor layer in retarding the heat transfer is still strongly felt. Finally, contact boiling occurs when  $T_s \sim T_{SL}$  and  $\xi_s \sim 10^3$  m/s<sup>2</sup>. Within this regime, the effect of the vapor layer has been completely suppressed, leading to higher CER values ( $1.95 < \text{CER} < 2.05$ ).

## 5 Acknowledgments

The authors gratefully acknowledge receipt of funding for this work from the Fundamental Research Grant Scheme, Ministry of Higher Education Malaysia, through Project Grant No. FRGS/1/2013/SG02/MUSM/02/2 and the financial support from Green Electronics, Advanced Engineering Platform, Monash University Malaysia.

## References

- 1 J. G. Leidenfrost, *International Journal of Heat and Mass Transfer*, 1966, **9**, 1153 – 1166.
- 2 B. S. Gottfried, C. J. Lee and K. J. Bell, *International Journal of Heat and Mass Transfer*, 1966, **9**, 1167 – 1188.
- 3 D. Quéré, *Annual Review of Fluid Mechanics*, 2013, **45**, 197–215.
- 4 D. Quéré and A. Ajdari, *Nature Materials*, 2006, **5**, 429–430.
- 5 G. Lagubeau, M. L. Merrer, C. Clanet and D. Quéré, *Nature Physics*, 2011, **7**, 395–398.
- 6 T. Baier, G. Dupeux, S. Herbert, S. Hardt and D. Quéré, *Physical Review E*, 2013, **87**, 021001.
- 7 S. Hardt, S. Tiwari and T. Baier, *Physical Review E*, 2013, **87**, 063015.
- 8 I. U. Vakarelski, J. O. Marston, D. Y. C. Chan and S. T. Thoroddsen, *Physical Review Letters*, 2011, **106**, 214501.
- 9 H. Kim, B. Truong, J. Buongiorno and L.-W. Hu, *Applied Physics Letters*, 2011, **98**, 083121.
- 10 H.-M. Kwon, J. C. Bird and K. K. Varanasi, *Applied Physics Letters*, 2013, **103**, 201601.
- 11 R. C. A. van der Veen, M. H. W. Hendrix, T. Tran, C. Sun, P. A. Tsai and D. Lohse, *Soft Matter*, 2014, **10**, 3703–3707.
- 12 C. Kruse, T. Anderson, C. Wilson, C. Zuhlke, D. Alexander, G. Gogos and S. Ndao, *Langmuir*, 2013, **29**, 9798–9806.
- 13 C. M. Weickgenannt, Y. Zhang, S. Sinha-Ray, I. V. Roisman, T. Gambaryan-Roisman, C. Tropea and A. L. Yarin, *Physical Review E*, 2011, **84**, 036310.
- 14 H. Nair, H. J. J. Staat, T. Tran, A. van Houselt, A. Prosperetti, D. Lohse and C. Sun, *Soft Matter*, 2014, **10**, 2102–2109.
- 15 R. P. Sahu, S. Sinha-Ray, A. L. Yarin and B. Pourdeyhimi, *Soft Matter*, 2012, **8**, 3957–3970.
- 16 S. Jun, S. Sinha-Ray and A. L. Yarin, *International Journal of Heat and Mass Transfer*, 2013, **62**, 99 – 111.
- 17 S. Sinha-Ray and A. L. Yarin, *International Journal of Heat and Mass Transfer*, 2014, **70**, 1095 – 1106.
- 18 S. Sinha-Ray, S. Sinha-Ray, A. L. Yarin, C. M. Weickgenannt, J. Emmert and C. Tropea, *International Journal of Heat and Mass Transfer*, 2014, **70**, 1107 – 1114.
- 19 H. Kim, J. Buongiorno, L.-W. Hu and T. McKrell, *International Journal of Heat and Mass Transfer*, 2010, **53**, 1542 – 1553.
- 20 F. Celestini and G. Kirstetter, *Soft Matter*, 2012, **8**, 5992–5995.
- 21 W. Deng and A. Gomez, *Physics of Fluids*, 2010, **22**, 051703.

- 
- 22 T. Tran, H. J. J. Staat, A. Prosperetti, C. Sun and D. Lohse, *Physical Review Letters*, 2012, **108**, 036101.
  - 23 C. Clanet, C. Béguin, D. Richard and Q. David, *Journal of Fluid Mechanics*, 2004, **517**, 199–208.
  - 24 T. Tran, H. J. J. Staat, A. Susarrey-Arce, T. C. Foertsch, A. van Houselt, H. J. G. E. Gardeniers, A. Prosperetti, D. Lohse and C. Sun, *Soft Matter*, 2013, **9**, 3272–3282.
  - 25 P. Tsai, M. H. W. Hendrix, R. R. M. Dijkstra, L. Shui and D. Lohse, *Soft Matter*, 2011, **7**, 11325–11333.
  - 26 C. Antonini, I. Bernagozzi, S. Jung, D. Poulikakos and M. Marengo, *Physical Review Letters*, 2013, **111**, 014501.
  - 27 M. K. Koch, A. Voßnacke, J. Starflinger, W. Schütz and H. Unger, *Journal of Aerosol Science*, 2000, **31**, 1015–1028.
  - 28 F. MacIntyre, *The Journal of Physical Chemistry*, 1968, **72**, 589–592.
  - 29 L. Duchemin, S. Popinet, C. Josserand and S. Zaleski, *Physics of Fluids*, 2002, **14**, 3000–3008.
  - 30 H. K. Forster and N. Zuber, *AIChE Journal*, 1955, **1**, 531–535.
  - 31 A. M. K. H. Chaves and F. Obermeier, *International Journal of Heat and Fluid Flow*, 1999, **20**, 470–476.